SUPPLEMENTAL INFORMATION

Hemodynamic response function (HRF) variability confounds resting-state fMRI functional connectivity

D Rangaprakash[1,2], Guo-Rong Wu[3,4], Daniele Marinazzo[3], Xiaoping Hu[5], Gopikrishna Deshpande[1,6,7,8]

[1] AU MRI Research Center, Department of Electrical and Computer Engineering, Auburn University, Auburn, AL, USA.

[2] Department of Psychiatry and Biobehavioral Sciences, University of California Los Angeles, Los Angeles, CA, USA

[3] Department of Data Analysis, University of Ghent, Ghent, Belgium

[4] Key Laboratory of Cognition and Personality, Southwest University, Chongqing, China

[5] Department of Bioengineering, University of California Riverside, Riverside, CA, USA

[6] Department of Psychology, Auburn University, Auburn, AL, USA

[7] Center for Health Ecology and Equity Research, Auburn University, Auburn, AL, USA

[8] Alabama Advanced Imaging Consortium, Auburn University and University of Alabama Birmingham, AL, USA

S1. Construct validity of the deconvolution technique

The deconvolution technique's original paper [1] has presented several simulations illustrating the validity of the technique. Here, we provide two sanity checks for providing further validation of the deconvolution procedure. First, a fundamental claim of deconvolution is that if a pair of time series have identical HRFs, then their correlation would be the same with or without deconvolution, and that the deconvolution approach should be able to re-identify the correlation between the underlying neural event time series. Second, if two time series have different HRFs then the deconvolution approach should be able to accurately access the true neural correlation, but analysis without deconvolution would not. We performed simple simulations to demonstrate the construct validity of the deconvolution technique based on the above principles.

We chose a single fixed HRF from our data as the reference HRF. We started with the deconvolved data, and convolved each time series with the same reference HRF, simulating the scenario of pairs of time series having identical HRFs. We called the resulting data as the homogenously re-convolved (HR) data. We then computed the pairwise correlation between all the time series pairs for the non-deconvolved (NDC) data, as well as the HR data. In theory, the NDC and HR data must be identical, and these two correlation data must also be identical. However, in practice these would not be identical since deconvolution is not a noiseless process. To quantify the degree of similarity between the two correlations, we computed the percentage similarity between them as one minus the ratio of difference in correlation values to the correlation values of deconvolved data.

$$Percentage\ similarity\ between\ C^{NDC}\ and\ C^{HR} = \left(1 - \frac{\sum_{i=1}^{N}\sum_{j=1}^{N}\left(c_{i,j}^{NDC} - c_{i,j}^{HR}\right)}{\sum_{i=1}^{N}\sum_{j=1}^{N} c_{i,j}^{NDC}}\right) \times 100$$

Where, C^{NDC} is the correlation (or functional connectivity [FC]) matrix for NDC data with elements $c_{i,j}^{NDC}$, and C^{HR} is the correlation matrix for HR data with elements $c_{i,j}^{HR}$, with *(i,j)* corresponding to the connection between *region-i* and *region-j*, and *N* being the total number of regions. Higher the percentage, more identical are the NDC and HR correlations. We found the percentage similarity to be 99.673%. This finding demonstrates the credibility of the deconvolution technique employed in this work.

Next, to study the case of different HRFs, we chose a single fixed time series (*L*) from our deconvolved data (i.e. latent neural signal) as the reference time series. The correlation of this time

series with itself would be equal to 1. We then convolved this time series with all the HRFs derived from our entire data set (i.e. voxel-level HRF, denoted as *HRF(i,j,k)* where *i,j,k* denote the spatial location of the voxel in 3D co-ordinate space) to generate a new 4D data set of convolved time series (i.e. simulated raw BOLD data, denoted as *fMRI_sim(i,j,k,t)* where *t* represents time):

$$fMRI\_sim = L * HRF$$

Next, we performed deconvolution on each simulated fMRI time series to obtain estimated reference latent neural time series (denoted as *L'*) from the estimated HRF denoted as *HRF'*:

$$L' = HRF'^{-1} * fMRI\_sim$$

If the estimated (*L'*) and original (*L*) latent neural time series were identical, the correlation between the two (say, *K*) would be equal to 1, but since deconvolution is not noiseless we cannot expect that in practice. Performing this procedure and computing correlation between each estimated latent neural time series and the corresponding original time series in the data, we found that the mean correlation value (mean of *K*) was 0.99364 (standard deviation=0.00349). These findings show that both in the case of identical and different HRFs, the deconvolution procedure performs impressively, providing construct validity for the method.

S2. Simulations: The effect of sampling rate (TR) on FC-HRF relationship

We performed simulations for different sampling rates (TR) of 0.5, 1, 1.5 and 2 s, but the simulation results presented in the main document (**Fig.3**) were for TR=1s, because our experimental data had the same TR. However, for the sake of completeness, here we present and discuss the results across all TRs. **Fig.S1** shows plots similar to Fig.3, except that each plot has 4 separate lines representing different TRs. We found no significant impact of TR on any of these relationships, except with FWHM at 1 s (**Fig.S1c**). Nonetheless, longer TRs consistently resulted in a trend of higher connectivity error (ΔFC) throughout. This provides empirical evidence that the HRF parameters have nearly identical impact on FC at different TRs. Future studies could probe the impact of TR on FC-HRF relationship using experimental data.

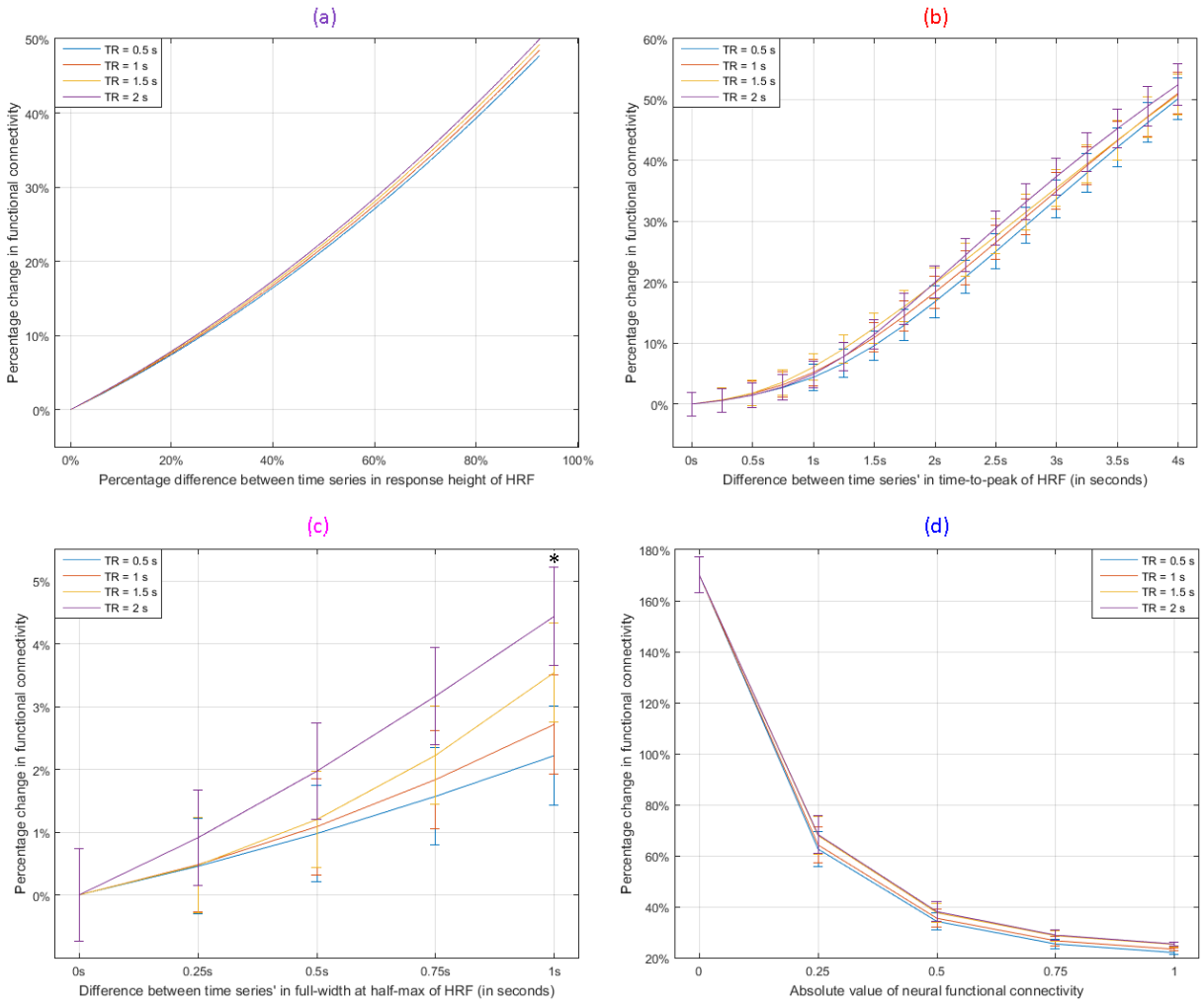

Fig.S1. *Simulation results for empirical assessment of percentage change in functional connectivity (ΔFC) between neural and BOLD time series caused by difference in HRF parameters (ΔRH, ΔTTP, ΔFWHM) between the corresponding two time series, across all possible physiologically plausible values of these HRF measures. The results are presented for 4 different sampling rate (TR) values: 0.5, 1, 1.5 and 2 s. A similar figure in the main document (Fig.3) presented results only for TR=1 s.* ***(a)*** *ΔFC vs. ΔRH (RH resolution=0.25%).* ***(b)*** *ΔFC vs. ΔTTP (TTP resolution=0.25s).* ***(c)*** *ΔFC vs. ΔFWHM (FWHM resolution=0.25s).* ***(d)*** *ΔFC vs. absolute value of neural FC (FC resolution=0.25). Error bars show one standard deviation above and below the mean. Figure-a does not show error bars since the error bars would mask the mean curve if used; nonetheless, the standard deviations are nearly identical to the ones visible in Fig.3a. The physiologically plausible lower and upper bounds of HRF parameters were obtained from* [2]. *There was no significant impact of TR, except with FWHM at 1s (corrected $p<0.05$). We*

observed robust and nearly linear positive relationship between ΔFC and change in HRF parameters. Up to 50% change in FC was observable due to either RH or TTP variability. Also smaller FC values were more vulnerable to HRF variability. RH=response height, TTP=time-to-peak, FWHM=full-width at half-max, FC=functional connectivity, TR=repetition time.

S3. Results: The ROIs and the table of p-values

Table S1. *The 58 ROIs of the default mode network used in this work, which was adopted from Power et al* [3]. *The MNI coordinates of each ROI are provided, along with ROI name obtained from Talairach Daemon (http://www.talairach.org/daemon.html). Each ROI was defined as a sphere of radius 5mm around the centroid of each ROI. Averaged timeseries obtained from all voxels in each ROI were used for further analysis.*

ROI	X	Y	Z	ROI name		
1	-41	-75	26	Middle Temporal Gyrus	Occipital_Mid_L (aal)	O.Mid.L
2	6	67	-4	undefined	Frontal_Med_Orb_R (aal)	F.Med.Orb.R
3	8	48	-15	Medial Frontal Gyrus	Rectus_R (aal)	Rectus.R
4	-13	-40	1	Parahippocampa Gyrus	Precuneus_L (aal)	Prec.L
5	-18	63	-9	Superior Frontal Gyrus	Frontal_Sup_Orb_L (aal)	F.Sup.Orb.L
6	-46	-61	21	Middle Temporal Gyrus	Temporal_Mid_L (aal)	T.Mid.L
7	43	-72	28	Middle Temporal Gyrus	Occipital_Mid_R (aal)	O.Mid.R
8	-44	12	-34	Superior Temporal Gyrus	Temporal_Pole_Mid_L (aal)	T.Pole.Mid.L
9	46	16	-30	Superior Temporal Gyrus	Temporal_Pole_Mid_R (aal)	T.Pole.Mid.R
10	-68	-23	-16	undefined	Temporal_Mid_L (aal)	T.Mid.L
11	-44	-65	35	Angular Gyrus	Angular_L (aal)	Angular.L
12	-39	-75	44	undefined	Angular_L (aal)	Angular.L
13	-7	-55	27	Cingulate Gyrus	Precuneus_L (aal)	Prec.L
14	6	-59	35	Precuneus	Precuneus_R (aal)	Prec.R
15	-11	-56	16	Posterior Cingulate	Precuneus_L (aal)	Prec.L
16	-3	-49	13	Posterior Cingulate	Precuneus_L (aal)	Prec.L
17	8	-48	31	Cingulate Gyrus	Cingulum_Mid_R (aal)	Cing.Mid.R
18	15	-63	26	Precuneus	Precuneus_R (aal)	Prec.R

19	-2	-37	44	Cingulate Gyrus	Cingulum_Mid_L (aal)	Cing.Mid.L
20	11	-54	17	Posterior Cingulate	Precuneus_R (aal)	Prec.R
21	52	-59	36	Angular Gyrus	Angular_R (aal)	Angular.R
22	23	33	48	Middle Frontal Gyrus	Frontal_Sup_R (aal)	F.Sup.R
23	-10	39	52	Superior Frontal Gyrus	Frontal_Sup_Medial_L (aal)	F.Sup.Med.L
24	-16	29	53	Superior Frontal Gyrus	Frontal_Sup_L (aal)	F.Sup.L
25	-35	20	51	Middle Frontal Gyrus	Frontal_Mid_L (aal)	F.Mid.L
26	22	39	39	Superior Frontal Gyrus	Frontal_Sup_R (aal)	F.Sup.R
27	13	55	38	Superior Frontal Gyrus	Frontal_Sup_R (aal)	F.Sup.R
28	-10	55	39	Superior Frontal Gyrus	Frontal_Sup_L (aal)	F.Sup.L
29	-20	45	39	Superior Frontal Gyrus	Frontal_Sup_L (aal)	F.Sup.L
30	6	54	16	Medial Frontal Gyrus	Frontal_Sup_Medial_R (aal)	F.Sup.Med.R
31	6	64	22	Medial Frontal Gyrus	Frontal_Sup_Medial_R (aal)	F.Sup.Med.R
32	-7	51	-1	Medial Frontal Gyrus	Cingulum_Ant_L (aal)	Cing.Ant.L
33	9	54	3	Medial Frontal Gyrus	Frontal_Sup_Medial_R (aal)	F.Sup.Med.R
34	-3	44	-9	Medial Frontal Gyrus	Frontal_Med_Orb_L (aal)	F.Med.Orb.L
35	8	42	-5	Medial Frontal Gyrus	Frontal_Med_Orb_R (aal)	F.Med.Orb.R
36	-11	45	8	Medial Frontal Gyrus	Cingulum_Ant_L (aal)	Cing.Ant.L
37	-2	38	36	Medial Frontal Gyrus	Frontal_Sup_Medial_L (aal)	F.Sup.Med.L
38	-3	42	16	Anterior Cingulate	Cingulum_Ant_L (aal)	Cing.Ant.L
39	-20	64	19	Superior Frontal Gyrus	Frontal_Sup_L (aal)	F.Sup.L
40	-8	48	23	Medial Frontal Gyrus	Frontal_Sup_Medial_L (aal)	F.Sup.Med.L
41	65	-12	-19	Inferior Temporal Gyrus	Temporal_Mid_R (aal)	T.Mid.R
42	-56	-13	-10	Middle Temporal Gyrus	Temporal_Mid_L (aal)	T.Mid.L
43	-58	-30	-4	Middle Temporal Gyrus	Temporal_Mid_L (aal)	T.Mid.L
44	65	-31	-9	Middle Temporal Gyrus	Temporal_Mid_R (aal)	T.Mid.R
45	-68	-41	-5	Middle Temporal Gyrus	Temporal_Mid_L (aal)	T.Mid.L
46	13	30	59	Superior Frontal Gyrus	Frontal_Sup_Medial_R (aal)	F.Sup.Med.R
47	12	36	20	Anterior Cingulate	Cingulum_Ant_R (aal)	Cing.Ant.R
48	52	-2	-16	Middle Temporal Gyrus	Temporal_Mid_R (aal)	T.Mid.R
49	-26	-40	-8	Parahippocampa Gyrus	ParaHippocampal_L (aal)	ParaHipp.L
50	27	-37	-13	Parahippocampa Gyrus	Fusiform_R (aal)	Fusiform.R
51	-34	-38	-16	Fusiform Gyrus	Fusiform_L (aal)	Fusiform.L
52	28	-77	-32	Uvula	Cerebelum_Crus1_R (aal)	Cerebel.Crus1.R
53	52	7	-30	Middle Temporal Gyrus	Temporal_Pole_Mid_R (aal)	T.Pole.Mid.R

54	-53	3	-27	Middle Temporal Gyrus	Temporal_Mid_L (aal)	T.Mid.L
55	47	-50	29	Supramarginal Gyrus	Angular_R (aal)	Angular.R
56	-49	-42	1	Middle Temporal Gyrus	Temporal_Mid_L (aal)	T.Mid.L
57	-46	31	-13	Inferior Frontal Gyrus	Frontal_Inf_Orb_L (aal)	F.Inf.Orb.L
58	49	35	-12	Inferior Frontal Gyrus	Frontal_Inf_Orb_R (aal)	F.Inf.Orb.R

Table S2. *Significant connections (p<0.05, Bonferroni corrected) with functional connectivity being higher with deconvolved data compared to non-deconvolved data (pseudo negatives). The MNI coordinates and names of the corresponding ROIs can be obtained from Table S1.*

Connection		**p-value**			
ROI #1	**ROI #2**	**FC**	**HRF - RH**	**HRF-FWHM**	**HRF - TTP**
53	13	$7.7x10^{-06}$	$2.3x10^{-16}$	$2.1x10^{-86}$	$1.1x10^{-79}$
53	26	$2.9x10^{-05}$	$6.6x10^{-13}$	$1.2x10^{-125}$	$1.6x10^{-119}$
53	27	$6.9x10^{-06}$	$1.7x10^{-08}$	$1.1x10^{-120}$	$3.9x10^{-112}$
53	28	$2.2x10^{-05}$	$1.1x10^{-08}$	$1.4x10^{-125}$	$4.1x10^{-125}$
53	32	$1.9x10^{-08}$	$3.5x10^{-10}$	$1.8x10^{-120}$	$3.1x10^{-116}$
54	3	$3.9x10^{-06}$	$2.6x10^{-09}$	$2.3x10^{-123}$	$2.4x10^{-119}$
54	46	$3.3x10^{-07}$	$8.4x10^{-08}$	$3.1x10^{-47}$	$2.7x10^{-39}$
56	53	$2.6x10^{-05}$	$8.8x10^{-17}$	$1.8x10^{-121}$	$6.5x10^{-114}$

Table S3. *Significant connections (p<0.05, Bonferroni corrected) with functional connectivity being higher with non-deconvolved data compared to deconvolved data (pseudo positives). The MNI coordinates and names of the corresponding ROIs can be obtained from Table S1.*

Connection		**p-value**			
ROI #1	**ROI #2**	**FC**	**HRF - RH**	**HRF-FWHM**	**HRF - TTP**
5	30	$2.4x10^{-07}$	$5.7x10^{-20}$	$4.3x10^{-139}$	$5.4x10^{-129}$
5	36	$3.9x10^{-06}$	$3.0x10^{-28}$	$4.4x10^{-84}$	$8.9x10^{-77}$
5	44	$1.6x10^{-05}$	$1.0x10^{-25}$	$5.0x10^{-50}$	$3.4x10^{-48}$
5	46	$9.2x10^{-09}$	$2.0x10^{-21}$	$1.0x10^{-88}$	$4.0x10^{-79}$

5	47	$1.2x10^{-05}$	$1.2x10^{-31}$	$3.1x10^{-86}$	$4.9x10^{-76}$
6	30	$1.3x10^{-05}$	$1.3x10^{-25}$	$1.6x10^{-141}$	$3.2x10^{-128}$
6	32	$6.3x10^{-07}$	$2.6x10^{-09}$	$3.5x10^{-48}$	$9.0x10^{-40}$
6	36	$2.4x10^{-05}$	$1.1x10^{-31}$	$3.6x10^{-91}$	$1.4x10^{-81}$
6	46	$8.6x10^{-06}$	$1.4x10^{-26}$	$7.9x10^{-96}$	$1.2x10^{-83}$
7	8	$1.4x10^{-07}$	$1.5x10^{-18}$	$2.7x10^{-141}$	$4.2x10^{-120}$
7	34	$4.2x10^{-06}$	$2.4x10^{-29}$	$1.3x10^{-130}$	$2.3x10^{-112}$
7	46	$5.7x10^{-10}$	$1.9x10^{-17}$	$3.3x10^{-68}$	$1.2x10^{-54}$
7	47	$6.2x10^{-07}$	$2.3x10^{-30}$	$5.9x10^{-62}$	$1.8x10^{-47}$
8	13	$3.5x10^{-06}$	$2.6x10^{-21}$	$3.8x10^{-142}$	$5.7x10^{-132}$
8	36	$1.1x10^{-06}$	$5.0x10^{-07}$	$3.1x10^{-121}$	$7.4x10^{-114}$
8	47	$8.7x10^{-08}$	$1.0x10^{-10}$	$7.9x10^{-133}$	$3.5x10^{-121}$
9	36	$1.4x10^{-06}$	$4.6x10^{-24}$	$5.3x10^{-42}$	$4.3x1^{0-39}$
9	46	$2.2x10^{-08}$	$6.6x10^{-16}$	$3.0x10^{-46}$	$1.5x10^{-42}$
11	46	$6.1x10^{-07}$	$1.3x10^{-17}$	$2.0x10^{-96}$	$9.4x10^{-84}$
13	34	$1.5x10^{-05}$	$3.7x10^{-31}$	$2.8x10^{-133}$	$3.6x10^{-125}$
13	46	$2.6x10^{-12}$	$2.4x10^{-20}$	$1.4x10^{-88}$	$1.0x10^{-80}$
13	47	$1.3x10^{-05}$	$4.5x10^{-32}$	$4.9x10^{-86}$	$9.0x10^{-78}$
34	44	$6.7x10^{-09}$	$5.0x10^{-06}$	$3.2x10^{-124}$	$4.7x10^{-122}$
34	46	$3.6x10^{-09}$	$2.4x10^{-13}$	$1.1x10^{-115}$	$5.9x10^{-106}$

S4. Does spatial smoothing affect the results?

In our original pre-processing pipeline, we included spatial smoothing with an 8mm Gaussian kernel. We wanted to test whether non-smoothed data generated different results. In order to do so, we repeated the entire analysis using data without spatial smoothing. However, we did not find any significant differences in the HRF maps between the smoothed and non-smoothed data.

This could be due to the following reasons: (i) The variability of the HRF parameters across neighboring voxels is considerably lower than the variability in the BOLD signal, activation or other BOLD-derived metrics [2]. In addition, time-to-peak and FWHM of the HRF are not continuous variables but quantized metrics with the smallest unit being 1 TR (in seconds), hence their variability around the vicinity of a given voxel is very low. Thus, smoothing may not cause

drastic changes in the HRF parameters, except likely in boundary regions. (ii) This study considered regions-of-interest (ROIs) and performed ROI-to-ROI connectivity among all ROIs, while comparing the corresponding ROI HRFs. This choice was grounded again on the evidence that the variability of HRF parameters within the few voxels of a functional ROI (for the ROI size we have used) is considerably low. The ROI HRFs were averaged across the voxels within the ROI; hence, given that this has an effect equivalent to smoothing or spatial low-pass filtering, the additional step of smoothing may have had minimal impact.

As alternatives to ROI-based analysis, performing pairwise voxel-level connectivity modeling with the whole brain is computationally prohibitively intensive, while performing seed-to-whole-brain connectivity modeling would lead to the challenge of choosing a specific seed, which is arbitrary when considering a healthy control population as in our study. Nonetheless, regardless of the cause, the data revealed no significant differences in the findings between smoothed and non-smoothed fMRI data.

S5. Does deconvolution introduce higher frequencies into the deconvolved signal?

Could the deconvolution process result in deconvolved data having higher frequency components, which can then drive differences between deconvolved and non-deconvolved data? To test this, we obtained the power spectra of fMRI time series before and after deconvolution for all voxels in the brain for all the subjects. We then defined the -20dB bandwidth for each spectrum, having lower and upper cut-off boundaries defined by when the spectrum falls by 20dB (=by 100 times) relative to the peak of the spectrum. We then collected all the lower and upper cut-off frequencies for data before and after deconvolution, and performed statistical comparison (t-test) between them to test for any differences in low (and high) frequency content between the two sets. We found no significant differences (see **Fig.S2**) between deconvolved and non-deconvolved data ($p>0.05$), implying that lower (and higher) frequency content was not introduced into the data by performing deconvolution. This suggests that deconvolution does not significantly alter the spectral characteristics of the signal.

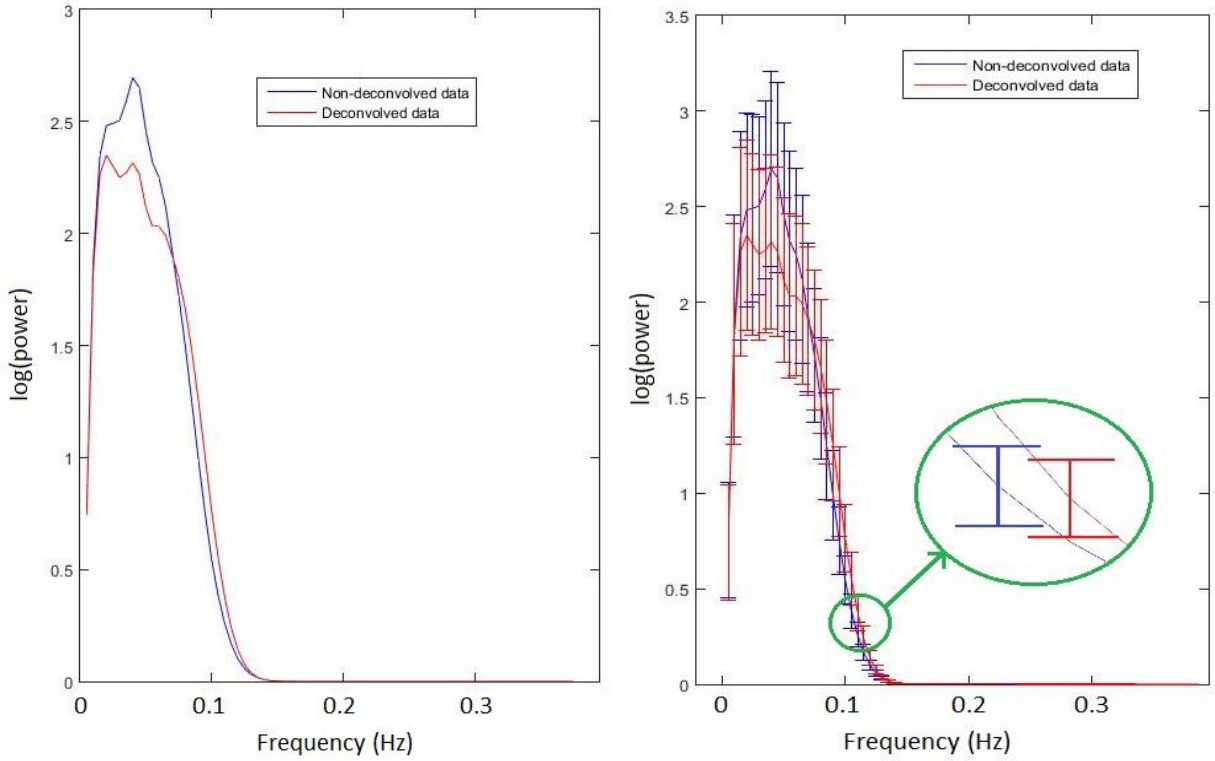

(a) **(b)**

Fig.S2. *Comparing the frequency spectra (power spectral density) of deconvolved and non-deconvolved data, obtained from the entire data set. (a) Mean spectra: we noticed them to be nearly overlapping. (b) Spectra with standard deviations, along with the zoomed inlet showing the location of -20 dB upper cut-off power (100 times attenuation with respect to the peak). We can observe that the standard deviations were large compared to mean difference at that point, which is why they were not significant (p>0.05). The two spectra were found to not differ.*

SUPPLEMENTAL REFERENCES

[1] G. Wu, W. Liao, S. Stramaglia, J. Ding, H. Chen and D. Marinazzo, "A blind deconvolution approach to recover effective connectivity brain networks from resting state fMRI data," *Med Image Anal.* , vol. 17, no. 3, pp. 365-374, 2013.

[2] D. A. Handwerker, J. M. Ollinger and M. D'Esposito, "Variation of BOLD hemodynamic responses across subjects and brain regions and their effects on statistical analyses," *Neuroimage,* vol. 21, no. 4, pp. 1639-51, 2004.

[3] J. D. Power, A. L. Cohen, S. M. Nelson, G. S. Wig and K. A. Barnes, "Functional network organization of the human brain," *Neuron,* vol. 72, no. 4, pp. 665-78, 2011.

[4] G. Deshpande, K. Sathian and X. Hu, "Assessing and compensating for zero-lag correlation effects in time-lagged Granger causality analysis of FMRI," *IEEE Transactions on Biomedical Engineering,* vol. 57, no. 6, pp. 1446-56, 2010.

[5] C. Granger, "Investigating causal relations by econometric models and cross-spectral methods," *Econometrica,* vol. 37, pp. 424-438, 1969.

[6] K. Friston, J. Ashburner, S. Kiebel, T. Nichols and W. Penny, Statistical Parametric Mapping: The Analysis of Functional Brain Images, Academic Press, 2007.

[7] A. Roebroeck, E. Formisano and R. Goebel, "Mapping directed influence over the brain using Granger causality and fMRI," *Neuroimage,* vol. 25, no. 1, pp. 230-242, 2005.

[8] N. Logothetis, J. Pauls, M. Augath, T. Trinath and A. Oeltermann, "Neurophysiological investigation of the basis of the fMRI signal," *Nature,* vol. 412, pp. 150-157, 2001.